LOCAL FIELD ASSESSMENT INSIDE MULTISCALE COMPOSITE ARCHITECTURES*

TIMOTHY BREITZMAN†, ROBERT LIPTON‡, AND ENDEL IARVE§

Abstract. We introduce asymptotic expansions for recovering the local field behavior inside multiscale composite architectures in the presence of residual stress. The theory applies to zones containing abrupt changes in the composite microgeometry. This includes the interfaces between plies inside fiber reinforced laminates. The asymptotic expansions are used to develop a fast numerical algorithm to extract local field information inside a prescribed subdomain without having to resort to a full numerical simulation. For regions of homogeneous microstructure, the analysis delivers bounds on the magnitude of the local stress and strain fields inside the composite. Numerical examples are provided to demonstrate the utility of the asymptotic theory for quickly assessing the location and magnitude of local field concentrations inside complex composite architectures.

Key words. corrector theory, fiber reinforced composites, stress analysis

AMS subject classifications.

1. Introduction.

The new generation of high performance composites features a hierarchy of substructures deployed across several length scales [35]. These include advanced composite architectures made from woven fiber tows and fiber reinforced laminates. These architectures are characterized by abrupt changes in the microstructure at the interface between substructural units. Understanding the behavior of local stress and strain fields across these regions is necessary for quantifying failure initiation inside composite structures. In this paper we employ suitable asymptotic expansions to develop algorithms useful for the numerical simulation of local fields across interfaces where the microstructure changes abruptly.

The last several years has seen the introduction and rapid development of sophisticated multiscale approaches for the numerical modeling of fields inside composites and heterogeneous media. Some recent reviews and foundational work in this rapidly growing literature are presented in [1, 7, 10, 13, 14, 15, 18, 21, 22, 23, 24, 35, 39, 40, 41, 44, 46, 48]. All multiscale methods naturally employ some form of local enhancement of the approximation space in order to capture the higher frequency oscillations arising from material heterogeneity. These methods, although not based upon homogenization theory, can, in some cases, be motivated by the intrinsic multiscale construction used in the homogenization method [3], [8], and [45]. It is anticipated that the methods developed in this paper will provide motivation for selecting local approximation spaces useful for local FEM enhancement across prestressed zones over which the microstructure changes rapidly.

The approach developed here applies to composite materials with residual stress and is tailored to resolve field behavior across regions where there is abrupt variation in the local microgeometry. The numerical method developed in this paper provides

* Research supported by NSF Grant DMS-0406374 and Air Force Grants FA9550-05-0008, FA9550-04-1-0142 and the Boeing Aircraft Company. **To Appear in Multiscale Modeling and Simulation, 2007.**

†Air Force Research Laboratory, Wright Patterson AFB, OH 45433,(timothy.breitzman@wpafb.af.mil).

‡Department of Mathematics, Louisiana State University, Baton Rouge, LA 70803, (lipton@math.lsu.edu).

§300 College Park, University of Dayton Research Institute, Dayton, OH 45469, (endel.iarve@wpafb.af.mil).

a fast way to extract local field information inside prescribed subdomains without having to resort to a full numerical simulation. The numerical method is compared to a direct numerical simulation for a symmetric three ply laminate in Section 4. For subregions containing a fixed periodic microstructure such as the interior of a ply or woven tow, our approach delivers asymptotically tight upper bounds on the magnitude of the local stress and strain fields inside these regions. The bounds are shown to hold when the microstructure is sufficiently small relative to the characteristic length scale of the ply width or tow diameter. The upper bounds are computed for selected plies inside a symmetric eight ply laminate perforated by a circular hole in Section 5. The bounds provide a quick and numerically inexpensive means to examine the effect of residual stress inside composite structures.

The asymptotic expansions developed here are seen to converge in the point wise sense see, Section 3. However, in this article we do not give estimates for the convergence rates of these expansions in terms of L^p or sup norms. For the fiber reinforced laminates studied here it is important to note that the rate of convergence depends upon the penetration of the boundary layers near free edges and in the vicinity of ply interfaces, [4], [9], [37], and [38]. Additionally the presence of local field concentrations generated by irregularities such as inclusions with sharp corners can foil any attempt at establishing uniform convergence [17], [29], [31], [34], [36]. The effects of the boundary layer are discussed in Section 4 where a direct numerical simulation is carried out for a symmetric three ply laminate. For this example the fibers are arranged periodically inside each ply and each ply is six period cells thick. The top and bottom plies have long cylindrical fibers oriented with generators parallel to the x axis. The middle ply has fibers oriented with generators along the y axis. The plies are infinite in extent along the x direction and twenty periods wide along the y direction and the laminate is subjected to a 1% strain in the x direction see, Figure 4.2. The simulations show that the asymptotic theory captures the trends up to about one fiber diameter away from the free edge see, Figure 4.4 and the discussion in Section 4. However the error between the asymptotic expansions and the direct numerical simulation should increase for more general types of fiber distributions due the enhanced penetration of boundary layer effects associated with the free edge [6].

The presence of residual stress inside composite materials is an important factor that influences the processing and design of structural components [11], [12], [27], and [28]. Its effects are spread across several length scales, the smallest being the fiber-matrix length scale, the next being the inter laminar length scale and the largest being the structural length scale. The net result of these effects can be seen in the warpage of autoclaved composite parts [2]. The recent work of [47] models each ply as a homogeneous orthotropic material and examines the effect of fiber prestress at inter laminar length scales while the numerical and experimental work presented in [5] details the effects of residual stress at the fiber-matrix length scale. The numerical analysis presented in Section 5 is in some sense complementary to these efforts. In Section 5 we consider the combined effects of residual stress at the fiber-matrix length scale and at the inter laminar length scale and present a numerical procedure to resolve the local strain field at the fiber-matrix length scale inside each ply. The simulations are carried out for an eight ply symmetric laminate. The first simulation in Section 5 characterizes the local hydrostatic strain in the absence of residual stress, see Figures 5.11, 5.13, 5.15, while the second is carried out in the presence of residual stress due to matrix shrinkage after curing, see Figures 5.12, 5.14, 5.16.

Earlier related work focuses on developing suitable theoretical methods for the

assessment of local stress and strain fields inside non prestressed heterogeneous media. The work of [32], [33] develops rigorous upper bounds on local stress invariants in the general context of G-convergence by exploiting the differentiability of G-limits. A formal notion of quantities similar to correctors has recently been applied to analyze local fields in the neighborhood of microscopic stress concentrations [16, 25, 42]. For prestressed elastic composites, a formal procedure has been developed for field approximation inside zones containing a fixed periodic microstructure in [20]. The asymptotic expansions given in Theorem 3.2 provide the rigorous context for the multiscale arguments given in [20].

The paper is organized as follows: In Section 2, we review the homogenization theory relating average (macroscopic) stresses to average (macroscopic) strains inside prestressed multi-phase elastic composites. In Section 3, we develop the asymptotic analysis through the introduction of suitable corrector problems. In Section 4, we construct high fidelity asymptotic expansions for composite laminates and develop a computational method for local field recovery. The method is compared to direct numerical simulation for a three ply laminate and is found to capture the trends seen in the direct numerical simulation at a fraction of the computational cost. For subregions containing a fixed periodic microsturcture, the asymptotic analysis is used to develop upper bounds on the magnitude of the local stress and strain fields inside the composite, see Section 5. The bounds are computed numerically for the local strain inside an eight ply laminate perforated by a circular hole. The proofs of the asymptotic expansions are provided in Section 6. In this paper, all direct numerical simulations and computations based on asymptotic expansions are carried out using the B-Spline Analysis Method (BSAM) [26].

We conclude by introducing standard notation for representing products and contractions of tensors used in elasticity theory. The convention that repeated indices indicate summation is used throughout. Products of elastic tensors C and strain tensors e are written as $Ce = C_{ijkl}e_{kl}$, contractions of two second order tensors σ and e are written as $\sigma : e = \sigma_{ij}e_{ij}$, the norm of a second order tensor is $|e| = (e_{ij}^2)^{1/2}$, contraction of a second order tensor and a vector is written $e\mathbf{x} = e_{ij}x_j$ and tensor products of vectors $\mathbf{a}$ and $\mathbf{b}$ are denoted by $\mathbf{a} \otimes \mathbf{b} = a_i b_j$.

2. Homogenization. In this section, we provide a brief review of homogenization theory for prestressed composites. We consider a composite structure made from N different materials. Each material is characterized by its elastic tensor C^m as well as its stress free strain e^m, $m = 1, 2, \ldots, N$. In our context, the stress free strain accounts for the thermal expansion or contraction inside the m^{th} material due to a temperature change inside the structure. The elasticity tensor inside each phase satisfies the ellipticity and boundedness conditions given by $0 < \lambda|\eta|^2 < C^m\eta : \eta < \Lambda|\eta|^2$ for every constant 3×3 strain η and $0 < \lambda < \Lambda$. The multi-phase composite structure is contained inside a bounded domain in $\mathbf{R^3}$ denoted by Ω (see Figure 2.1). The structure is given by the union of several subdomains $\Omega_1, \Omega_2, \ldots, \Omega_L$ inside which the microstructure is periodic. Each subdomain is distinguished by the presence of a different periodic microstructure. This type of "locally periodic" microstructure is often used to describe the microstructure inside engineering composites such as fiber reinforced laminates and braided fiber reinforced composites. The characteristic length scale of the microstructure relative to the length scale of the subdomains is denoted by ϵ. The elasticity tensor for the composite structure is denoted by $C^\epsilon(\mathbf{x})$.

The elastic strain associated with the elastic displacement $\mathbf{u}^\epsilon$ is given by $e_{ij}(\mathbf{u}^\epsilon) = (u^\epsilon_{i,j} + u^\epsilon_{j,i})/2$. The stress free strain in the m^{th} material caused by thermal contraction

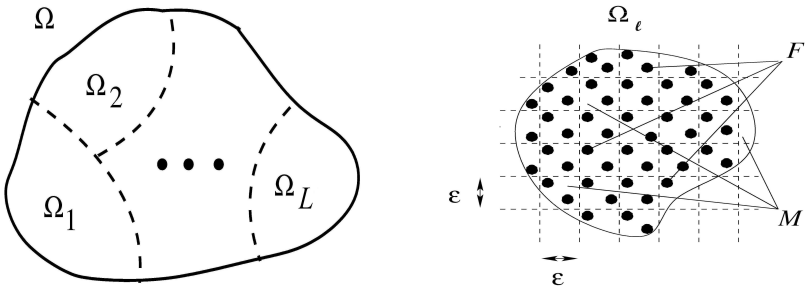

(a) Division of Domain Ω (b) General Subdomain Ω_ℓ of Ω

FIG. 2.1. *Cross-section of* Ω *and Subdomain* Ω_ℓ

or expansion due to an imposed temperature change $\triangle T$ is given by

$$e^m = \begin{bmatrix} \alpha_{11}^m \triangle T & 0 & 0 \\ 0 & \alpha_{22}^m \triangle T & 0 \\ 0 & 0 & \alpha_{33}^m \triangle T \end{bmatrix},$$

where α_{11}^m, α_{22}^m, α_{33}^m denote the coefficients of thermal expansion inside each phase $m = 1, 2, \ldots, N$. Here $\triangle T$ is assumed constant across the sample and the piecewise constant stress free strain inside the composite structure is denoted by $e^\epsilon(\mathbf{x})$. The stress inside the structure σ^ϵ is given by

$$\sigma_{ij}^\epsilon(\mathbf{x}) = C_{ijkl}^\epsilon(\mathbf{x}) \left(e_{kl}(\mathbf{u}^\epsilon)(\mathbf{x}) - e_{kl}^\epsilon(\mathbf{x}) \right). \tag{2.1}$$

The boundary of the structure Ω is split into two parts, Γ_D and Γ_N, where displacement and traction boundary conditions are prescribed. Here $\mathbf{u}^\epsilon = \mathbf{U}$ on Γ_D and $\sigma^\epsilon \mathbf{n} = \mathbf{g}$, on Γ_N, where $\mathbf{n}$ is the outward directed unit normal vector on Γ_N. The prescribed displacement and traction $\mathbf{U}$ and $\mathbf{g}$ are taken to be square integrable on Γ_D and Γ_N, respectively.

The elastic displacement inside the structure is square integrable and has square integrable derivatives and is the solution of the equilibrium equation

$$-\text{div} \left(C_{ijkl}^\epsilon(\mathbf{x}) \left(e_{kl}(\mathbf{u}^\epsilon)(\mathbf{x}) - e_{kl}^\epsilon(\mathbf{x}) \right) \right) = \mathbf{f}, \tag{2.2}$$

where the load $\mathbf{f}$ is taken to be square integrable. We interpret (2.2) in the weak sense, i.e.,

$$\int_\Omega \left(C_{ijkl}^\epsilon(\mathbf{x}) \left(e_{kl}(\mathbf{u}^\epsilon)(\mathbf{x}) - e_{kl}^\epsilon(\mathbf{x}) \right) \right) e_{ij}(\psi) \, d\mathbf{x} = \int_\Omega \mathbf{f} \cdot \psi \, d\mathbf{x} \tag{2.3}$$

for every smooth test function ψ that vanishes on the boundary of Ω. The weak formulation (2.3) implicitly accounts for perfect bonding transmission conditions between material phases. These are given by

$$\begin{aligned} \sigma_{|_a}^\epsilon \mathbf{n} &= \sigma_{|_b}^\epsilon \mathbf{n} \text{ and} \\ \mathbf{u}_{|_a}^\epsilon &= \mathbf{u}_{|_b}^\epsilon. \end{aligned} \tag{2.4}$$

Here, the subscripts a and b indicate the side of the two phase interface on which quantities are evaluated and $\mathbf{n}$ is the unit normal vector to the interface pointing into phase b. In this paper all equilibrium equations are understood in the weak sense.

To describe the homogenization theorem, we introduce the indicator functions χ_ℓ of the subdomains Ω_ℓ, $\ell = 1, \ldots, L$. Here, the indicator function χ_ℓ takes the value one for $\mathbf{x}$ in Ω_ℓ and zero outside. Inside each subdomain Ω_ℓ, we associate a unit periodic elasticity tensor denoted by $C_\ell(\mathbf{y})$ and a unit periodic stress free strain denoted by $e_\ell(\mathbf{y})$. Here, $\mathbf{y}$ is used to denote points inside the unit period cell Q and $C_\ell(\mathbf{y}) = C^m$ for $\mathbf{y}$ inside the m^{th} material, $m = 1, \ldots, N$. Similarly, $e_\ell(\mathbf{y}) = e^m$ for $\mathbf{y}$ inside the m^{th} material, $m = 1, \ldots, N$. Setting

$$C(\mathbf{x}, \mathbf{y}) = \sum_{\ell=1}^{L} \chi_\ell(\mathbf{x}) C_\ell(\mathbf{y}), \tag{2.5}$$

the elasticity tensor for the composite structure is given by $C^\epsilon(\mathbf{x}) = C(\mathbf{x}, \mathbf{x}/\epsilon)$. Similarly, setting

$$e(\mathbf{x}, \mathbf{y}) = \sum_{\ell=1}^{L} \chi_\ell(\mathbf{x}) e_\ell(\mathbf{y}) \tag{2.6}$$

gives the stress free strain $e^\epsilon(\mathbf{x}) = e(\mathbf{x}, \mathbf{x}/\epsilon)$.

Next, we introduce the solutions of the periodic cell problems. Let $\mathbf{e}^1, \mathbf{e}^2, \mathbf{e}^3$ be an orthogonal system of unit vectors in $\mathbf{R^3}$. A basis for the set of constant 3×3 strains is given by $\overline{e}^{ij} = (\mathbf{e}^i \otimes \mathbf{e}^j + \mathbf{e}^j \otimes \mathbf{e}^i)/2$, $1 \le i \le j \le 3$. We introduce $\mathbf{w}^{ij}(\mathbf{x}, \mathbf{y})$, which is Q periodic in the $\mathbf{y}$ variable for every $\mathbf{x}$ in Ω, and is the solution of

$$\operatorname{div}\left(C(\mathbf{x}, \mathbf{y})\left(e(\mathbf{w}^{ij})(\mathbf{x}, \mathbf{y}) + \overline{e}^{ij}\right)\right) = 0, \tag{2.7}$$

where all derivatives are with respect to the $\mathbf{y}$ variable and $\mathbf{x}$ appears as a parameter.

The effective elastic tensor is defined by

$$C^E_{ijkl}(\mathbf{x}) = \int_Q \left(C_{ijmn}(\mathbf{x}, \mathbf{y})\left(e_{mn}(\mathbf{w}^{kl})(\mathbf{x}, \mathbf{y}) + \overline{e}^{ij}_{mn}\right)\right) d\mathbf{y}. \tag{2.8}$$

The effective thermal expansion coefficient is given by

$$H^E_{ij}(\mathbf{x}) = \int_Q C_{mnop}(\mathbf{x}, \mathbf{y})\left(e_{op}(\mathbf{w}^{ij})(\mathbf{x}, \mathbf{y}) + \overline{e}^{ij}_{op}\right) e_{mn}(\mathbf{x}, \mathbf{y}) d\mathbf{y}. \tag{2.9}$$

The homogenization of the prestressed multi-phase elastic problem is given by the following theorem [30].

THEOREM 2.1. Homogenization Theorem

For every choice of boundary data and right hand side, $\mathbf{u}^\epsilon \rightharpoonup \mathbf{u}^M$ weakly in $H^1(\Omega)^3$ as $\epsilon \to 0$. The convergence of the local stress is given by

$$\sigma^\varepsilon = C^\epsilon\left(e(\mathbf{u}^\epsilon) - e^\epsilon\right) \rightharpoonup \sigma^M = C^E_{ijkl} e_{kl}(\mathbf{u}^M) - H^E_{ij}, \tag{2.10}$$

weakly in $L^2(\Omega)^{3\times 3}$.

Moreover, $\mathbf{u}^M$ is the unique solution to the homogenized boundary value problem $\mathbf{u}^M = \mathbf{U}$ on Γ_D, $\sigma^M \mathbf{n} = \mathbf{g}$ on Γ_N and

$$-\operatorname{div}\left(C^E e(\mathbf{u}^M) - H^E\right) = \mathbf{f}. \tag{2.11}$$

The homogenization theory delivers the convergence of the local average stress and strain. Indeed, given any subset S contained inside Ω, one has that

$$\frac{1}{|S|}\int_S e(\mathbf{u}^\epsilon)d\mathbf{x} \to \frac{1}{|S|}\int_S e(\mathbf{u}^M)d\mathbf{x} \tag{2.12}$$

and

$$\frac{1}{|S|}\int_S \sigma^\epsilon d\mathbf{x} \to \frac{1}{|S|}\int_S \sigma^M d\mathbf{x}. \tag{2.13}$$

However, in order to characterize failure initiation inside the structure, one needs to extract information beyond that given by the asymptotics of averaged quantities. In the next section we present asymptotics that allow for the resolution of the local fields at the length scale of the microstructure.

3. High fidelity asymptotics for local field assessment. In this section, we present the asymptotic analysis for recovering the local field behavior inside multiscale prestressed composite architectures. The asymptotic theory is described in terms of the solution of auxiliary local boundary value problems. These boundary value problems are used to build a corrector theory suitable for capturing the multiscale coupling between the average fields and the local field fluctuations at the length scale of the microstructure. We prescribe a domain of interest S inside the composite structure. Here, the boundary of the set S does not intersect the boundary of Ω. Asymptotic expansions are developed that describe the local stress and strain fields inside S. It is important to point out that the microstructure contained inside S is not necessarily periodic. The utility of the expansion is that it applies to domains S that straddle interfaces separating two or more subdomains containing different periodic microstructures. The interface between the subdomains need not be straight or smooth. On the domain S, we introduce the $H_0^1(S)^3$ solutions $\mathbf{v}^{ij,\epsilon}$ and $\mathbf{r}^\epsilon$ of the multiscale equilibrium problems defined on S given by

$$-\text{div}\left(C^\epsilon(\mathbf{x})(e(\mathbf{v}^{ij,\epsilon})(\mathbf{x}) + \overline{e}^{ij})\right) = -\text{div}\left(C^E(\mathbf{x})\overline{e}^{ij}\right) \tag{3.1}$$

and

$$-\text{div}\left(C^\epsilon(\mathbf{x})(e(\mathbf{r}^\epsilon)(\mathbf{x}) - e^\epsilon(\mathbf{x}))\right) = \text{div}\left(H^E(\mathbf{x})\right). \tag{3.2}$$

The multiscale problem (3.1) is used to define the corrector tensor P^ϵ given by

$$P^\epsilon(\mathbf{x})\overline{e}^{ij} = e(\mathbf{v}^{ij,\epsilon})(\mathbf{x}) + \overline{e}^{ij}. \tag{3.3}$$

Here, the right hand sides of (3.1) and (3.2) record the effects of the interfaces separating subdomains containing different periodic microstructures.

The point wise convergence of the elastic stress and strain inside each phase is given by the following theorem.

THEOREM 3.1. Asymptotic expansion
Let $\chi_m^\epsilon(\mathbf{x})$ be the indicator function of the m^{th} material phase contained inside S where $\chi_m^\epsilon = 1$ for points inside the m^{th} phase and zero outside. On passage to a subsequence if necessary, one has the point wise asymptotics given by

$$\chi_m^\epsilon(\mathbf{x})\sigma^\epsilon(\mathbf{x}) - \chi_m^\epsilon(\mathbf{x})C^m\left(P^\epsilon(\mathbf{x})e(\mathbf{u}^M)(\mathbf{x}) + e(\mathbf{r}^\epsilon)(\mathbf{x}) - e^\epsilon(\mathbf{x})\right) \to 0, \tag{3.4}$$

$$\chi_m^\epsilon(\mathbf{x})e(\mathbf{u}^\epsilon)(\mathbf{x}) - \chi_m^\epsilon(\mathbf{x})\left(P^\epsilon(\mathbf{x})e(\mathbf{u}^M)(\mathbf{x}) + e(\mathbf{r}^\epsilon)(\mathbf{x}))\right) \to 0, \tag{3.5}$$

for $m = 1, \ldots, N$. Here the convergence is point wise and holds for almost every $\mathbf{x}$ *in* S.

When the set of interest is contained inside one of the subdomains, i.e., $S \subset \Omega_\ell$ the microstructure is periodic and the field interactions simplify. The point wise asymptotics can be expressed in terms of auxiliary problems posed over unit cells. For this case, let $\tilde{\mathbf{r}} = \tilde{\mathbf{r}}(\mathbf{y})$ be the periodic $H^1(Q)^3$ solution of

$$\text{div}\,(C_\ell(\mathbf{y})(e(\tilde{\mathbf{r}}) - e_\ell(\mathbf{y}))) = 0, \tag{3.6}$$

for $\mathbf{y}$ in Q, and let $\tilde{\mathbf{w}}^{ij} = \tilde{\mathbf{w}}^{ij}(\mathbf{y})$ be the periodic $H^1(Q)^3$ solution of

$$\text{div}\left(C_\ell(\mathbf{y})(e(\tilde{\mathbf{w}}^{ij}) + \overline{e}^{ij})\right) = 0, \tag{3.7}$$

for $\mathbf{y}$ in Q.

We extend $\tilde{\mathbf{w}}^{ij}$ and $\tilde{\mathbf{r}}$ by periodicity to $\mathbf{R^3}$. The corrector tensor $\tilde{P} = \tilde{P}(\mathbf{y})$ is given by

$$\tilde{P}(\mathbf{y})\overline{e}^{ij} = e(\tilde{\mathbf{w}}^{ij})(\mathbf{y}) + \overline{e}^{ij} \tag{3.8}$$

and we set $\tilde{P}^\epsilon(\mathbf{x}) = \tilde{P}(\mathbf{x}/\epsilon)$ and $\tilde{\mathbf{r}}^\epsilon = \epsilon\tilde{\mathbf{r}}(\mathbf{x}/\epsilon)$. For this case, we note that $e(\tilde{\mathbf{r}}^\epsilon)(\mathbf{x}) = e(\tilde{\mathbf{r}})(\mathbf{x}/\epsilon)$ The point wise convergence of the elastic stress and strain inside each phase is given by the following theorem.

THEOREM 3.2. Asymptotic expansion for periodic microstructure with prestress *On passage to a subsequence if necessary, the point wise asymptotic behavior is given by*

$$\chi_m^\epsilon(\mathbf{x})\sigma^\epsilon(\mathbf{x}) - \chi_m^\epsilon(\mathbf{x})C^m\left(\tilde{P}(\mathbf{x}/\epsilon)e(\mathbf{u}^M)(\mathbf{x}) + e(\tilde{\mathbf{r}})(\mathbf{x}/\epsilon) - e^\epsilon(\mathbf{x})\right) \to 0, \tag{3.9}$$

$$\chi_m^\epsilon(\mathbf{x})e(\mathbf{u}^\epsilon)(\mathbf{x}) - \chi_m^\epsilon(\mathbf{x})\left(\tilde{P}(\mathbf{x}/\epsilon)e(\mathbf{u}^M)(\mathbf{x}) + e(\tilde{\mathbf{r}})(\mathbf{x}/\epsilon))\right) \to 0, \tag{3.10}$$

for $m = 1, \ldots, N$. Here the convergence is point wise and holds for almost every $\mathbf{x}$ *in* S.

Theorem 3.2 is known at least by experts. For the analogous scalar problem in the more general setting of oscillating applied forces the corrector results corresponding to Theorem 3.2 are established in [43]. In the context of Theorem 3.2 the earlier work of [45] provides formal asymptotic expansions for elastically homogeneous media with an oscillatory applied force.

It should be emphasized that Theorems 3.1 and 3.2 are presented in the general setting where the oscillating elastic coefficients are only assumed to be measurable. Thus one is only able to claim point wise almost every where convergence of the expansions. In this context the coefficients may correspond to nonsmooth included phases or other geometries that contain stress or strain singularities. For these cases there are always points where the convergence is violated.

The proofs of theorems 3.1 and 3.2 are provided in Section 6.

4. Multiscale field assessment inside prestressed fiber reinforced laminates using high fidelity asymptotics. Theorem (3.1) accounts for the effects of longer length scales due to the variation of microstructure between subdomains. In the context of fiber reinforced laminates, the domain $\Omega = \cup_{\ell=1}^L \Omega_\ell$ can be thought of

as a stack of plies. In this example, each ply is of uniform thickness and is denoted by Ω_ℓ. We consider the case when the set of interest S is a pillbox straddling the interface between two adjacent plies Ω_ℓ, $\Omega_{\ell+1}$, see Figure 4.1. Each ply contains a periodic array of long parallel fibers running the length of the ply. The fiber orientation is different for each ply. The fibers are separated by a second connected phase called the matrix material. The elasticity and stress free strain for the matrix material is given by C^1 and e^1. To fix ideas, we assume that all fibers have the same elastic tensor and stress free strain specified by C^2 and e^2. For this case, the solution $\mathbf{v}^{ij,\epsilon}$ of the auxiliary problem (3.1) satisfies

$$\begin{aligned} -\text{div}\left(C_\ell(\mathbf{x}/\epsilon)(e(\mathbf{v}^{ij,\epsilon})(\mathbf{x})+\overline{e}^{ij})\right)=0,\ \text{for } \mathbf{x}\in S\cap\Omega_\ell \\ -\text{div}\left(C_{\ell+1}(\mathbf{x}/\epsilon)(e(\mathbf{v}^{ij,\epsilon})(\mathbf{x})+\overline{e}^{ij})\right)=0,\ \text{for } \mathbf{x}\in S\cap\Omega_{\ell+1}, \end{aligned} \tag{4.1}$$

and on the boundary separating $S\cap\Omega_\ell$ and $S\cap\Omega_{\ell+1}$, $\mathbf{v}^{ij,\epsilon}$ satisfies the transmission condition

$$\mathbf{v}^{ij,\epsilon}_{|_\ell}=\mathbf{v}^{ij,\epsilon}_{|_{\ell+1}}, \tag{4.2}$$

and

$$\begin{aligned} &\left(C_\ell(\mathbf{x}/\epsilon)(e(\mathbf{v}^{ij,\epsilon})(\mathbf{x})+\overline{e}^{ij})-C^E(\mathbf{x})\overline{e}^{ij}\right)_{|_\ell}\mathbf{n} \\ &=\left(C_{\ell+1}(\mathbf{x}/\epsilon)(e(\mathbf{v}^{ij,\epsilon})(\mathbf{x})+\overline{e}^{ij})-C^E(\mathbf{x})\overline{e}^{ij}\right)_{|_{\ell+1}}\mathbf{n}, \end{aligned} \tag{4.3}$$

where $\mathbf{n}$ is the normal on the interface pointing into $\Omega_{\ell+1}$ and the subscripts indicate the side of the interface on which quantities are evaluated. For this case, the solution $\mathbf{r}^\epsilon$ of (3.2) satisfies

$$\begin{aligned} -\text{div}\left(C_\ell(\mathbf{x}/\epsilon)(e(\mathbf{r}^\epsilon)(\mathbf{x})-e_\ell(\mathbf{x}/\epsilon))\right)=0,\ \text{for } \mathbf{x}\in S\cap\Omega_\ell \\ -\text{div}\left(C_{\ell+1}(\mathbf{x}/\epsilon)(e(\mathbf{r}^\epsilon)(\mathbf{x})-e_{\ell+1}(\mathbf{x}/\epsilon))\right)=0,\ \text{for } \mathbf{x}\in S\cap\Omega_{\ell+1}, \end{aligned} \tag{4.4}$$

and on the boundary separating $S\cap\Omega_\ell$ and $S\cap\Omega_{\ell+1}$, one has the transmission conditions

$$\mathbf{r}^{ij,\epsilon}_{|_\ell}=\mathbf{r}^{ij,\epsilon}_{|_{\ell+1}} \tag{4.5}$$

and

$$\begin{aligned} &\left(C_\ell(\mathbf{x}/\epsilon)(e(\mathbf{r}^\epsilon)(\mathbf{x})-e_\ell(\mathbf{x}/\epsilon))+H^E(\mathbf{x})\right)_{|_\ell}\mathbf{n} \\ &=\left(C_{\ell+1}(\mathbf{x}/\epsilon)(e(\mathbf{r}^\epsilon)(\mathbf{x})-e_\ell(\mathbf{x}/\epsilon))+H^E(\mathbf{x})\right)_{|_{\ell+1}}\mathbf{n}. \end{aligned} \tag{4.6}$$

The point wise asymptotics for the stress σ^ϵ and strain $e(\mathbf{u}^\epsilon)$ inside the pillbox S are described by (3.4) and (3.5) and are given in terms of the local solutions of the transmission problems (4.1 – 4.3) and (4.4 – 4.6). These asymptotics take into account the effects occurring at longer length scales due to the residual stresses and the elastic interaction between neighboring plies.

4.1. High fidelity asymptotics and a computational method for field recovery: a case study. In this section, we consider a symmetric three ply laminate. Here, the top and bottom plies contain a periodic arrangement of cylindrical fibers with generators oriented along the $\mathbf{x}$ axis (0° fiber orientation) and the middle ply contains a periodic arrangement of cylindrical fibers with generators oriented along

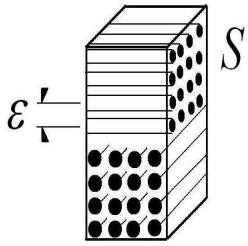

FIG. 4.1. *A domain of interest S containing the interface between two plies.*

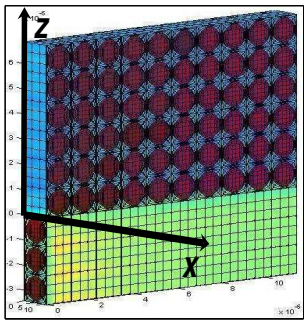

FIG. 4.2. *One slice of a quarter section of a three ply laminate. The slice is one period thick along the* **x** *axis*

the **y** axis (90° fiber orientation). This three ply laminate is referred to as a $[0, 90, 0]$ laminate. The laminate is made from IM7 Carbon fibers and 5250-4 Epoxy matrix. The associated elastic properties and coefficients of thermal expansion (CTE) for the fibers and matrix obtained from [42] are listed in Table 4.1. The fiber volume fraction of the IM7/5250-4 composite is 60%.

	IM7 Fiber	5250-4 Epoxy Matrix
E_{11}	276 GPa	3.45 GPa
E_{22}, E_{33}	27.6 GPa	3.45 GPa
ν_{12}, ν_{13}	0.3	0.35
ν_{23}	0.8	0.35
G_{12}, G_{13}	138 GPa	1.28 GPa
G_{23}	7.67 GPa	1.28 GPa
α_{11}	$-0.36 \times 10^{-7}/^\circ$ C	$46.8 \times 10^{-6}/^\circ$ C
α_{22}, α_{33}	$5.04 \times 10^{-6}/^\circ$ C	$46.8 \times 10^{-6}/^\circ$ C

TABLE 4.1
Elastic moduli and CTE for IM7 Fiber and 5250-4 Epoxy Matrix

We consider an infinitely long three ply laminate. The laminate is loaded with an imposed 1% strain along the **x** axis and the sides are kept traction free. A direct numerical simulation is carried out for the [0,90,0] laminate. Here, the 0 degree plies consist of stacks of 6 fibers through the thickness and twenty of these stacks are are placed side by side along the **y** direction. The 90 degree ply consists of stacks of

six fibers through the thickness and this stack is periodically repeated along the $\mathbf{x}$ direction see, Figure 4.2. In what follows we describe dimensions of length relative to the length of the period cell for the periodic geometry. With this convention, the y coordinate ranges from $y = 0$ at the free edge to $y = 10$ at the center of the laminate, see Figure 4.2. In what follows, we will use the results of the direct numerical simulation to compute the J_2 invariant of the local strain inside the 0° and 90° plies near the interface. These results will be compared to the J_2 invariant of the first two terms of the asymptotic expansion (3.5) computed over pre-selected subdomains of interest. Here, the J_2 invariant of the local strain tensor is given by

$$J_2(e(\mathbf{u}^\varepsilon(\mathbf{x}))) = \sqrt{\frac{3}{2}}\sqrt{|e(\mathbf{u}^\varepsilon(\mathbf{x}))|^2 - \frac{(\mathrm{tr}(e(\mathbf{u}^\varepsilon(\mathbf{x})))^2}{3}}, \tag{4.7}$$

where $|e(\mathbf{u}^\varepsilon(\mathbf{x}))|^2 = \sum_{i,j=1}^3 (e(\mathbf{u}^\varepsilon(\mathbf{x})))_{ij}^2$. Our choice of the J_2 invariant for the strain tensor is motivated by a recently proposed strain invariant failure theory for composite materials given in [20].

In the following examples, we will take the domain of interest S to lie across the interface and contain a single fiber cross section in the 0 degree ply above the interface and a single fiber cross section below the interface inside the 90 degree ply as shown in Figure 4.3. This choice of S is referred to in Figure 4.4 as an "Interface Cell".

In what follows, we start by choosing S next to the free edge with its center at the coordinates $x = 0.5, y = 0.5, z = 0$. For this choice we compute the first two terms of the asymptotic expansion. Then we shift S one period to the right of the free edge along the $\mathbf{y}$ axis and again compute the first two terms. This is done for $y = 1.5, 2.5, \ldots, 9.5$. For each choice of S, we compute the maximum of the J_2 invariant of the sum of the two terms in the high fidelity asymptotic expansion taken over the upper half of S inside the epoxy in the 0 degree ply. For this computation we have used $e(\mathbf{u}^M)$ evaluated at the upper boundary of the ply interface for $y = 0.5, 1.5, 2.5, \ldots, 9.5$. The associated step function curve is denoted by $M^0(y)$ and is plotted for $0 < y < 10$ and is the third curve from the bottom in Figure 4.4. We also compute the maximum of the J_2 invariant of the sum of the first two terms in the asymptotic expansion over the lower half of S inside the epoxy phase in the 90 degree ply. Here $e(\mathbf{u}^M)$ is evaluated at the lower boundary of the ply interface for $y = 0.5, 1.5, 2.5, \ldots, 9.5$. The associated step function curve $M^{90}(y)$ is the fifth curve up from the bottom plotted in Figure 4.4. The J_2 curves derived from the direct numerical simulation in the 90 degree middle ply and top 0 degree ply are given by the top curve and the bottom curve in Figure 4.4 respectively. To illustrate how these curves are computed we express the dependence of J_2 on position and write $J_2 = J_2(x, y, z)$ where $z = 0$ is the ply interface and $y = 0$ corresponds to the free edge. For $x = 0.5$ and for each y, $(0 < y < 10)$, the top curve is the graph of $M_d^{90}(y)$ which is given by the maximum of J_2 inside the epoxy matrix taken over $-1 < z < 0$ see, Figure 4.2. Here

$$M_d^{90}(y) = \max\{J_2(0.5, y, z); -1 < z < 0, (0.5, y, z) \text{ inside the epoxy}\} \tag{4.8}$$

and is plotted for $0 \le y \le 10$. Similarly the the bottom curve $M_d^0(y)$ is the maximum over $0 < z < 1$ of $J_2(0.5, y, z)$ inside the epoxy given by

$$M_d^0(y) = \max\{J_2(0.5, y, z); 0 < z < 1, (0.5, y, z) \text{ inside the epoxy}\} \tag{4.9}$$

and is plotted for $0 \le y \le 10$.

We start by comparing the M_d^{90} curve obtained from direct numerical simulation with the step curve M^{90}. Figure 4.4 shows that the M^{90} and M_d^{90} curves coincide up to about one fiber diameter away from the free edge. The primary reason for their disagreement is that the M_d^{90} curve captures the free edge singularity at the fiber matrix interface in the 90 degree ply, while the value of $e(\mathbf{u}^M)$ used for calculating M^{90} is never closer than one half period away from the free edge and thus remains finite. For this case the high fidelity asymptotic analysis compares well with the direct numerical simulation up to about one fiber diameter away from the free edge.

Next, we compare the direct numerical simulation with the high fidelity expansion inside the 0 degree ply. The curve M^0 associated with the high fidelity expansion lies above the curve M_d^0 associated with the direct numerical simulation in the 0 degree ply. The M^0 curve is seen to recover the local maxima appearing in the M_d^0 curve up to about two periods away from the free edge.

The M_d^0 and M_d^{90} curves illustrate the penetration of the free edge effects into the interior of the 0 and 90 degree ply. It is seen that the M_d^{90} curve is flat after six periods and the M_d^0 curve becomes periodic only after seven periods away from the free edge.

It is pointed out that ϵ for this problem is taken to be the ratio of the ply thickness to the fiber period and is given by $1/6$. However is anticipated that for this choice of ϵ that the error between the asymptotics and direct numerical simulation will increase for less regular fiber distributions. Moreover it is anticipated that the boundary effects associated with the free edge would penetrate further into the interior of the laminate for less regular fiber configurations [6].

For comparison, we also plot the J_2 curves associated with the two scale asymptotic expansion (3.10) when S is taken to be a period cell lying completely inside either the 0 degree ply or the 90 degree ply (these are referred to as Ply RVE's in Figure 4.4). We start with S next to the free edge with its center at the coordinates $x = 0.5, y = 0.5, z = 0.5$ and then compute the maximum value of J_2 over the epoxy phase inside S. Then we repeat this with S shifted to the right for $y = 1.5, 2.5, \ldots, 9.5$. The associated step function curve is the second curve from the bottom in Figure 4.4. It is seen from the figure that this curve significantly underestimates M_d^0 as given by the bottom curve in Figure 4.4. The corresponding J_2 curve associated with S inside the 90 degree ply is given by the fourth curve up from the bottom in Figure 4.4. This curve captures the trend seen in the M_d^0 curve until about one fiber diameter from the free edge.

These examples show the utility of the high fidelity expansions for capturing trends seen in regions containing rapid variation of local microstructure. It also underscores the importance of choosing the proper domain of interest S for computing asymptotic expansions inside regions where the microstructure changes abruptly.

5. Bounds on local stress and strain invariants. In this section, we provide a description of the local field behavior inside regions containing uniform microstructure, such as the interior of a ply inside a multi-ply laminate. We display upper bounds on the magnitude of the J_1 and J_2 invariants of the local stress and strain fields inside the composite. These bounds are rigorously shown to hold when the microstructure is sufficiently small relative to the characteristic length scale of the ply width. These bounds provide for the fast assessment of effects due to prestress inside multiscale composite architectures containing stress concentrations such as bolt holes. We illustrate this by computing the strain bounds inside selected plies for multi-ply fiber reinforced laminates.

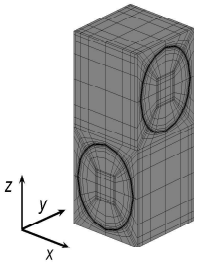

FIG. 4.3. *The choice of S used for computation of the high fidelity asymptotic expansion.*

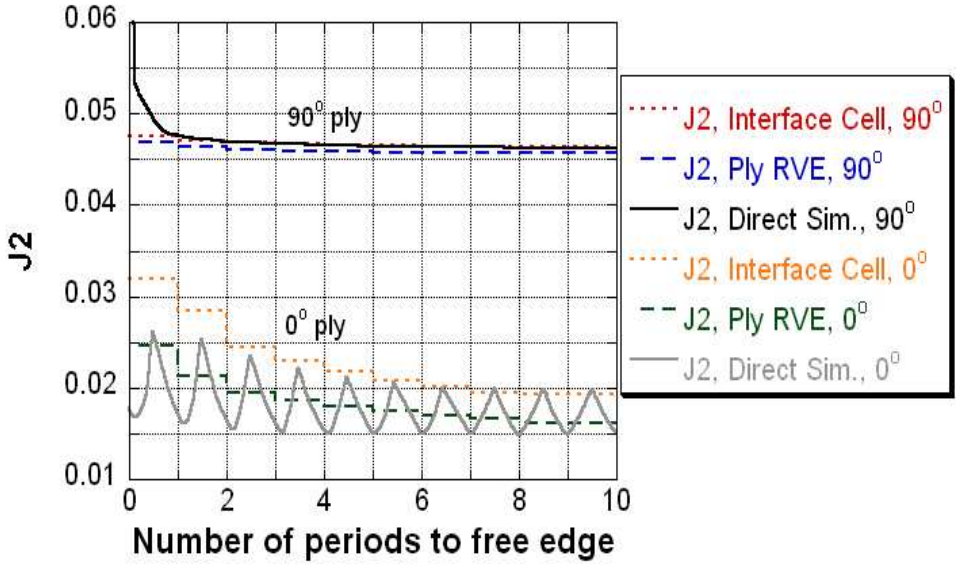

FIG. 4.4. *Comparison between direct numerical simulation and high fidelity asymptotitcs.*

To fix ideas, we consider a ply Ω_ℓ inside the laminate containing a fixed periodic microstructure. The unit periodic elasticity tensor and stress free strain for the microsturcture inside the ℓ^{th} ply are denoted by $C_\ell(\mathbf{y})$ and $\eta_\ell(\mathbf{y})$, respectively. Here, we recall that the J_1 invariant of a second order tensor τ is its trace, i.e.,

$$J_1(\tau) = \mathrm{tr}(\tau) = \sum_{i=1}^{3} \tau_{ii}. \tag{5.1}$$

We now give the point wise bounds on the J_1 and J_2 stress and strain invariants inside a ply. Let χ_m denote the indicator function of the m^{th} phase inside the unit period cell for the microstructure and we introduce $(SJ_1)_m$ and $(SJ_2)_m$, $m = 1, 2$, given by

$$(SJ_1)_m(\sigma^M) = \sup_{\mathbf{y}\in Q} J_1\left(\chi_m(\mathbf{y})C_\ell(\mathbf{y})(\tilde{P}(\mathbf{y})e^M + e(\tilde{\mathbf{r}})(\mathbf{y}) - \eta_\ell(\mathbf{y}))\right) \tag{5.2}$$

and

$$(SJ_2)_m(\sigma^M) = \sup_{\mathbf{y}\in Q} J_2\left(\chi_m(\mathbf{y})C_\ell(\mathbf{y})(\tilde{P}(\mathbf{y})e^M + e(\tilde{\mathbf{r}})(\mathbf{y}) - \eta_\ell(\mathbf{y}))\right). \tag{5.3}$$

The length scale of the microstructure relative to the length scale of the ply is denoted by ϵ and the local stress for the laminate inside the ply of interest is denoted by σ^ϵ. The indicator function for the m^{th} phase inside the ply is written as χ_m^ϵ.

Stress bound

Fix $\delta > 0$. Then for almost every $\mathbf{x}$ inside the ply, there is an $\epsilon_0 > 0$ such that, for $\epsilon < \epsilon_0$, one has that

$$\begin{aligned}&\chi_m^\epsilon(\mathbf{x})J_1(\sigma^\epsilon(\mathbf{x})) < (SJ_1)_m(\sigma^M(\mathbf{x})) + \delta \text{ and}\\ &\chi_m^\epsilon(\mathbf{x})J_2(\sigma^\epsilon(\mathbf{x})) < (SJ_2)_m(\sigma^M(\mathbf{x})) + \delta.\end{aligned} \tag{5.4}$$

We describe the strain bound in terms of $(EJ_1)_m$ and $(EJ_2)_m$, $m = 1, 2$, given by

$$(EJ_1)_m(e^M)) = \sup_{\mathbf{y}\in Q} J_1\left(\chi_m(\mathbf{y})(\tilde{P}(\mathbf{y})e^M + e(\tilde{\mathbf{r}})(\mathbf{y}) - \eta_\ell(\mathbf{y}))\right) \tag{5.5}$$

and

$$(EJ_2)_m(e^M) = \sup_{\mathbf{y}\in Q} J_2\left(\chi_m(\mathbf{y})(\tilde{P}(\mathbf{y})e^M + e(\tilde{\mathbf{r}})(\mathbf{y}) - \eta_\ell(\mathbf{y}))\right). \tag{5.6}$$

Strain bound

Fix $\delta > 0$. Then for almost every $\mathbf{x}$ inside the ply, there is an $\epsilon_0 > 0$ such that, for $\epsilon < \epsilon_0$, one has that

$$\begin{aligned}&\chi_m^\epsilon(\mathbf{x})J_1(e(\mathbf{u}^\epsilon(\mathbf{x}))) < (EJ_1)_m(e^M(\mathbf{x})) + \delta \text{ and}\\ &\chi_m^\epsilon(\mathbf{x})J_2(e(\mathbf{u}^\epsilon(\mathbf{x}))) < (EJ_2)_m(e^M(\mathbf{x})) + \delta.\end{aligned} \tag{5.7}$$

These bounds are established in Section 6.

It should be emphasized that the stress and strain bounds given here are presented in the general setting where the oscillating elastic coefficients are only assumed to be measurable. In this context the coefficients may correspond to nonsmooth included phases or other singular geometries. For these cases there are physically significant points where both the local stress and strain fields are infinite for every choice of ϵ. It is easily checked that the first term appearing in the upper bounds for the stress and strain fields is also infinite for every ϵ and for every point inside the ply for these cases. Thus the upper bounds on the stress and strain diverge to infinity when the microstructure supports stress or strain singularities.

In the following examples, we compare the strain bounds $(EJ_1)_1$ and $(EJ_2)_1$ with the strain invariants J_1 and J_2 obtained from direct numerical simulation. This comparison will be made for selected paths taken inside the 0 degree ply in the [0,90,0] symmetric three ply laminate introduced in Section 4. Here, it is stressed that the strain bounds hold only asymptotically; however, in the following example we will

compare them to the results of direct numerical simulation inside fiber reinforced composite geometries using material properties seen in the applications. We find that the strain bounds compare well to the direct numerical simulations.

We carry out the comparison by computing the J_1 and J_2 invariants using a full numerical simulation along four paths inside the 0 degree ply. The paths are taken 3.0, 2.5, 1.5 and 0.5 fiber diameters above the interface, respectively, and are illustrated in Figure 5.1. These paths lie inside the matrix phase. The strain bounds $(EJ_1)_1$ and $(EJ_2)_1$ inside the matrix phase are also computed along the paths. In the following figures, the strain bounds $(EJ_1)_1$ and $(EJ_2)_1$ are given by solid curves and J_1 and J_2 are given by dashed curves. Comparison of Figures 5.2, 5.4, 5.6, and 5.8 shows that $(EJ_1)_1$ is an upper bound for J_1 on all paths except within one fiber diameter of the free edge along the 0.5 fiber diameter path. It is seen from Figure 5.3 that $(EJ_2)_1$ is an upper bound for J_2 along the 3.0 fiber diameter path. However, for paths closer to the interface, $(EJ_2)_1$ is no longer an upper bound (see Figures 5.5, 5.7, and 5.9). This is due to the effect of the neighboring 90 degree ply on J_2 for paths close to the interface. On the other, hand we recall from Figure 4.4 that the high fidelity asymptotics developed using the domain of interest S straddling the interface was able to bound J_2 for any path chosen near the interface and up to one fiber diameter away from the free edge.

We conclude this section by computing the strain bound on J_1 inside the matrix material for a symmetric eight ply laminate containing an open circular hole. The laminate is made from IM7 fibers and 977-3 matrix. The associated elastic properties and coefficients of thermal expansion (CTE) for the fibers and matrix obtained from [20] are listed in Table 5.1. The fiber volume fraction of the IM7/977-3 composite is 60% and the ΔT used for the prestress is -150° C. The plies are stacked from top to bottom in the following sequence $[0^\circ, 45^\circ, -45^\circ, 90^\circ, 90^\circ, -45^\circ, 45^\circ, 0^\circ]$. Here, the angles represent the fiber orientation inside each ply. For this example, the ply thickness is 0.127 mm, and each ply has length 101.6 mm and width 25.4 mm, and the hole diameter is 6.35 mm (see Figure 5.10). The period cell for the fibers is $11.4 \times 10^{-3} mm$ and the fiber diameters are $10 \times 10^{-3} mm$. This multiscale structure contains roughly 1.8×10^6 fibers. From the previous numerical experiments, it was found that the strain bound held in regions greater than 3.0 fiber diameters from the ply interface. With this in mind, we will compute upper bounds along the mid plane of selected plies. Here, the mid plane is at least 5 fiber diameters away from the ply interface.

	IM7 Fiber	977-3 Matrix
E_{11}	271 GPa	3.79 GPa
E_{22}, E_{33}	17.2 GPa	3.79 GPa
ν_{12}, ν_{13}	0.32	0.36
ν_{23}	0.20	0.36
G_{12}, G_{13}	27.6 GPa	1.39 GPa
G_{23}	8.27 GPa	1.39 GPa
α_{11}	$-0.33 \times 10^{-6}/^\circ$ C	$17.7 \times 10^{-6}/^\circ$ C
α_{22}, α_{33}	$2.55 \times 10^{-6}/^\circ$ C	$17.7 \times 10^{-6}/^\circ$ C

TABLE 5.1
Elastic moduli and CTE for IM7 Fiber and 977-3 Matrix

We compute $(EJ_1)_1$ along the mid plane of the 0°, 45°, and 90° plies in the

presence of prestress and without prestress. Figure 5.11 is a contour plot of the strain bound $(EJ_1)_1$ inside the 0° ply in the absence of prestress and Figure 5.12 is the bound in the presence of prestress. Figure 5.13 is a plot of the strain bound $(EJ_1)_1$ inside the 45° ply in the absence of prestress and Figure 5.14 is the bound in the presence of prestress. Figure 5.15 is a plot of the strain bound $(EJ_1)_1$ inside the 90° ply in the absence of prestress and Figure 5.16 is the bound in the presence of prestress. It is clear from the Figures that the strain bounds in the presence of prestress are less symmetric than the strain bounds without prestress. This phenomenon is an inter laminar effect and is associated with the anisotropy of the off axis plies being more pronounced due to additional matrix contraction. These Figures illustrate the use of the strain bounds for uncovering phenomena due of the effect of prestress inside the eight ply laminate.

6. Proof of Theorem 3.1. In this section, we establish Theorem 3.1. We note that Theorem 3.2 holds for the simpler case of periodic microgeometries and its proof follows from the proof of Theorem 3.1. We point out that Theorem 3.2 is known at least by experts. For the analogous scalar problem in the more general setting of oscillating applied forces the corrector results corresponding to Theorem 3.2 are established in [43].

In what follows, we pass to limits of products of weakly converging sequences using compensated compactness. In the context of linear elasticity this is expressed in the following theorem [19].

THEOREM 6.1. Div-Curl Theorem for linear elasticity

1. *Suppose that* $\mathbf{v}^\epsilon \rightharpoonup \mathbf{v}$ *weakly in* $H^1(S)^3$,
2. $\eta^\epsilon \rightharpoonup \eta$ *weakly in* $L^2(S)^{3\times 3}$ *and*
3. $-div\, \eta^\epsilon = \mathbf{f}$, *with* $\mathbf{f} \in H^{-1}(S)^3$.

Then for every test function ϕ *in* $C_0^\infty(S)$,

$$\lim_{\epsilon\to 0}\int_S (e(\mathbf{v}^\epsilon) : \eta^\epsilon)\,\phi\, d\mathbf{x} \;=\; \int_S (e(\mathbf{v}) : \eta)\,\phi\, d\mathbf{x}.$$

We show that Theorem 3.1 follows from Theorem 6.1 together using the convergence properties of the auxiliary problems (3.1), (3.2). We note that Theorem 3.2 also follows from the same arguments and makes use of the convergence properties of the auxiliary problems (3.6), (3.7). We record these properties below.

$$\begin{aligned} \mathbf{v}^{ij,\epsilon} &\to 0, \text{ in } L^2(S)^3 \\ P^\epsilon \overline{e}^{ij} = e(\mathbf{v}^{ij,\epsilon}) + \overline{e}^{ij} &\rightharpoonup \overline{e}^{ij}, \text{ weakly in } L^2(S)^{3\times 3}, \\ C^\epsilon P^\epsilon \overline{e}^{ij} &\rightharpoonup C^E \overline{e}^{ij}, \text{ weakly in } L^2(S)^{3\times 3}, \text{ and} \end{aligned} \tag{6.1}$$

$$\begin{aligned} \mathbf{r}^\epsilon &\rightharpoonup 0, \text{ in } H_0^1(S)^3 \\ C^\epsilon(e(\mathbf{r}^\epsilon) - e^\epsilon) &\rightharpoonup -H^E, \text{ weakly in } L^2(S)^{3\times 3}. \end{aligned} \tag{6.2}$$

If $S \subset \Omega_\ell$, then

$$\begin{aligned} \epsilon\tilde{\mathbf{w}}^{ij}(\mathbf{x}/\epsilon) &\to 0, \text{ in } L^2(S)^3 \\ \tilde{P}^\epsilon \overline{e}^{ij} = e(\tilde{\mathbf{w}}^{ij})(\mathbf{x}/\epsilon) + \overline{e}^{ij} &\rightharpoonup \overline{e}^{ij}, \text{ weakly in } L^2(S)^{3\times 3}, \\ C^\epsilon \tilde{P}^\epsilon \overline{e}^{ij} &\rightharpoonup C^E \overline{e}^{ij}, \text{ weakly in } L^2(S)^{3\times 3}, \end{aligned} \tag{6.3}$$

$$\tilde{\mathbf{r}}^\epsilon \rightharpoonup 0, \text{ in } H^1(S)^3, \text{ and}$$
$$C^\epsilon(e(\tilde{\mathbf{r}}^\epsilon) - e^\epsilon) \rightharpoonup -H^E, \text{ weakly in } L^2(S)^{3\times 3}. \tag{6.4}$$

The convergence expressed in (6.1) and (6.3) follows from standard arguments, see [8]. The convergence of the auxilary problems (6.2) and (6.4) needs special treatment and are derived below. We establish (6.2), noting that (6.4) follows from a similar argument.

Proof of (6.2).

Standard estimates show that the sequences $\{\mathbf{r}^\epsilon\}_{\epsilon>0}$ and $C^\epsilon(e(\mathbf{r}^\epsilon) - e^\epsilon) = M^\epsilon$ are bounded in $H^1(S)^3$ and $L^2(S)^{3\times 3}$, respectively. On passage to subsequences if necessary, there exist $\bar{\mathbf{r}} \in H^1(S)^3$ and $M \in L^2(S)^{3\times 3}$ for which

$$\mathbf{r}^\epsilon \rightharpoonup \bar{\mathbf{r}} \quad \text{weakly in } H^1(S)^3, \tag{6.5}$$
$$M^\epsilon \rightharpoonup M \text{ weakly in } L^2(\Omega)^{3\times 3}, \text{ and} \tag{6.6}$$
$$-\operatorname{div} M = \operatorname{div} H^E. \tag{6.7}$$

We now show that $M = -H^E$. Given S, consider every subdomain Ω_ℓ that intersects S. For $\mathbf{x}$ inside such Ω_ℓ, we extend $\mathbf{w}^{ij}(\mathbf{x}, \mathbf{y})$ by periodicity to $\mathbf{R^3}$ in the $\mathbf{y}$ variable. Set $\Phi^\epsilon = \epsilon \mathbf{w}^{ij}(\mathbf{x}, \mathbf{x}/\epsilon) + \bar{e}^{ij}\mathbf{x}$ and note that

$$\operatorname{div}\,(C^\epsilon e(\Phi^\epsilon)) = 0 \tag{6.8}$$

on $\mathbf{R^3}$. For any test function δ in $C_0^\infty(\Omega_\ell \cap S)$, the product $\delta\Phi^\epsilon$ is an admissible test function for the weak formulation (3.2) and it follows that

$$\int_S (C^\epsilon(\mathbf{x})(e(\mathbf{r}^\epsilon)(\mathbf{x}) - e^\epsilon(\mathbf{x}))) : e(\delta\Phi^\epsilon)\, d\mathbf{x} = -\int_S H^E(\mathbf{x}) : e(\delta\Phi^\epsilon)\, d\mathbf{x}. \tag{6.9}$$

Expanding $\delta\Phi^\epsilon$ and regrouping terms in (6.9) gives

$$\begin{aligned}
&\int_S (C^\epsilon(\mathbf{x}) e(\Phi^\epsilon) : e(\mathbf{r}^\epsilon))\, \delta\, d\mathbf{x} - \int_S (C^\epsilon(\mathbf{x}) e(\Phi^\epsilon) : e^\epsilon)\, \delta\, d\mathbf{x} \\
&+ \int_S (C^\epsilon(\mathbf{x})(e(\mathbf{r}^\epsilon) - e^\epsilon))\, \nabla\delta\Phi^\epsilon\, d\mathbf{x} \\
&= -\int_S H^E(\mathbf{x}) : e(\delta\Phi^\epsilon)\, d\mathbf{x}.
\end{aligned} \tag{6.10}$$

Noting that oscillatory periodic functions weakly converge to their averages, [8] gives

$$\Phi^\epsilon \rightharpoonup \bar{e}^{ij}\mathbf{x} \qquad \text{weakly in } H^1(\Omega_\ell \cap S)^3, \tag{6.11}$$
$$C^\epsilon e(\Phi^\epsilon) \rightharpoonup C^E \bar{e}^{ij} \quad \text{weakly in } L^2(\Omega_\ell \cap S)^{3\times 3}, \text{ and} \tag{6.12}$$
$$C^\epsilon e(\Phi^\epsilon) : e^\epsilon \rightharpoonup H^E \bar{e}^{ij} \text{ weakly in } L^2(\Omega_\ell \cap S)^{3\times 3}. \tag{6.13}$$

Since (6.5), (6.8), and (6.12) hold, we apply the Div-curl lemma to the first term of (6.10) and applying (6.13) to the second term of (6.10) and taking limits in other terms using (6.6) and (6.11) gives

$$\begin{aligned}
&\int_S \left(C^E \bar{e}^{ij} : e(\bar{r})\right) \delta\, d\mathbf{x} - \int_S \left(H^E : \bar{e}^{ij}\right) \delta\, d\mathbf{x} \\
&+ \int_S M \nabla\delta \bar{e}^{ij}\mathbf{x}\, d\mathbf{x} \\
&= -\int_S H^E(\mathbf{x}) : e(\delta\bar{e}^{ij}\mathbf{x})\, d\mathbf{x}.
\end{aligned} \tag{6.14}$$

Applying the identity $M : e(\delta\overline{e}^{ij}\mathbf{x}) = M\nabla\delta\overline{e}^{ij}\mathbf{x} + M\overline{e}^{ij}\delta$ and recalling (6.7) gives

$$\int_S \left(M - C^E e(\overline{r}) + H^E\right)\overline{e}^{ij}\delta\, d\mathbf{x} = 0, \tag{6.15}$$

so $M = C^E e(\overline{r}) - H^E$ in S. From (6.7), it now follows that $\mathrm{div}(C^E e(\overline{r})) = 0$ and we conclude that $\overline{r} = 0$ to find that

$$M = -H^E. \tag{6.16}$$

Last, one recalls that the solution $\overline{r} \in H_0^1(S)$ of $\mathrm{div}(C^E e(\overline{r})) = 0$ is unique and it follows that the the whole sequence M^ϵ weakly converges to $-H^E$ in S. This concludes the proof of (6.2).

Theorem 3.1 will be established with the aid of an estimate described below. We introduce the matrix valued function $\overline{\varphi}$ defined by

$$\overline{\varphi} = \sum_{i,j=1}^{3} \overline{\varphi}_{ij}(x)\overline{e}^{ij}, \tag{6.17}$$

where $\overline{\varphi}_{ij}(x) \in C^\infty(\Omega)$ for every choice of i, j. The estimate is given by

THEOREM 6.2. Convergence estimate
Given a set of interest S, then for any open subset $\omega \subset\subset S$,

$$\limsup_{\epsilon\to 0} \int_\omega |e(\mathbf{u}^\epsilon) - (P^\epsilon\overline{\varphi} + e(\mathbf{r}^\epsilon))|^2 d\mathbf{x} \le \frac{\Lambda}{\lambda}\int_\omega |\left(e(\mathbf{u}^M) - \overline{\varphi}\right)|^2 d\mathbf{x}. \tag{6.18}$$

Proof of Theorem 3.1.

It is evident that if $e_{ij}(\mathbf{u}^M)$ is in $C^\infty(S)$, then setting $\overline{\varphi} = e(\mathbf{u}^M)$ in (6.18) gives the strong convergence

$$\lim_{\epsilon\to 0} \int_\omega |e(\mathbf{u}^\epsilon) - \left(P^\epsilon e(\mathbf{u}^M) + e(\mathbf{r}^\epsilon)\right)|^2 dx = 0. \tag{6.19}$$

More generally, one may consider the smooth approximation of $e(\mathbf{u}^M)$ in the $L^2(\Omega)^{3\times 3}$ norm denoted by $\overline{\varphi}$ in $C^\infty(S)^{3\times 3}$ such that

$$|\overline{\varphi} - e(\mathbf{u}^M)|_{L^2(S)^{3\times 3}} < \delta. \tag{6.20}$$

Applying Cauchy's inequality gives

$$\begin{aligned} &|P^\epsilon e(\mathbf{u}^M) - P^\epsilon\overline{\varphi}|_{L^1(S)^{3\times 3}} \\ &\le |\overline{\varphi} - e(\mathbf{u}^M)|_{L^2(S)^{3\times 3}} \left(\sum_{kl} |P^\epsilon\overline{e}^{kl}|_{L^2(S)^{3\times 3}}\right) \le \delta K, \end{aligned} \tag{6.21}$$

where K is a positive constant independent of ϵ. We write

$$e(\mathbf{u}^\epsilon) - \left(P^\epsilon e(\mathbf{u}^M) + e(\mathbf{r}^\epsilon)\right) = z_1^\epsilon + z_2^\epsilon, \tag{6.22}$$

where $z_1^\epsilon = e(\mathbf{u}^\epsilon) - (P^\epsilon\overline{\varphi} + e(\mathbf{r}^\epsilon))$ and $z_2^\epsilon = P^\epsilon\overline{\varphi} - P^\epsilon e(\mathbf{u}^M)$. From (6.18), (6.20), (6.21), and (6.22), we see that

$$\lim_{\epsilon\to 0} |e(\mathbf{u}^\epsilon) - \left(P^\epsilon e(\mathbf{u}^M) + e(\mathbf{r}^\epsilon)\right)|_{L^1(\omega)^{3\times 3}} < \delta(\frac{\Lambda}{\lambda} + K). \tag{6.23}$$

The point wise convergence given in (3.5) of Theorem 3.1 now follows immediately upon noting that δ can be chosen arbitrarily small.

In order to establish the convergence given by (3.4) of Theorem 3.1, we write

$$e(\mathbf{u}^\epsilon) = P^\epsilon e(\mathbf{u}^M) + e(\mathbf{r}^\epsilon) + z_s^\epsilon, \tag{6.24}$$

where $z_s^\epsilon \to 0$ in $L^1(S)^{3\times 3}$. Next, recall that $\sigma^\epsilon = C^\epsilon(e(\mathbf{u}^\epsilon) - e^\epsilon)$ and substitution of (6.24) shows that

$$\sigma^\epsilon = C^\epsilon(P^\epsilon e(\mathbf{u}^M) + e(\mathbf{r}^\epsilon) - e^\epsilon) + z_{st}^\epsilon, \tag{6.25}$$

where $z_{st}^\epsilon \to 0$ in $L^1(S)^{3\times 3}$ and (3.4) follows.

We now establish Theorem 6.2. To do this, we show for any $\mathrm{C}_0^\infty(S)$ function ϕ that

$$\begin{aligned}&\lim_{\epsilon\to 0}\int_S \phi C^\epsilon\left(e(\mathbf{u}^\epsilon) - (P^\epsilon\overline{\varphi} + e(\mathbf{r}^\epsilon))\right) : \left(e(\mathbf{u}^\epsilon) - (P^\epsilon\overline{\varphi} + e(\mathbf{r}^\epsilon))\right) d\mathbf{x}\\ &= \int_S \phi C^E\left(e(\mathbf{u}^M) - \overline{\varphi}\right) : \left(e(\mathbf{u}^M) - \overline{\varphi}\right) d\mathbf{x}.\end{aligned} \tag{6.26}$$

Theorem 6.2 follows from (6.26) since $\lambda \le C^\epsilon \le \Lambda$ and, for $\phi \ge 0$, one has

$$\begin{aligned}&\limsup_{\epsilon\to 0}\lambda\int_S \phi|(e(\mathbf{u}^\epsilon) - (P^\epsilon\overline{\varphi} + e(\mathbf{r}^\epsilon))\,|^2 d\mathbf{x}\\ &\le \int_S \phi C^E\left(e(\mathbf{u}^M) - \overline{\varphi}\right) : \left(e(\mathbf{u}^M) - \overline{\varphi}\right) dx\\ &\le \Lambda\int_S \phi|e(\mathbf{u}^M) - \overline{\varphi}|^2 d\mathbf{x}.\end{aligned} \tag{6.27}$$

To establish (6.26), we start with

$$\int_S \phi C^\epsilon(\mathbf{x})\left(e(\mathbf{u}^\epsilon) - (P^\epsilon\overline{\varphi} + e(\mathbf{r}^\epsilon))\right) : \left(e(\mathbf{u}^\epsilon) - (P^\epsilon\overline{\varphi} + e(\mathbf{r}^\epsilon))\right) d\mathbf{x}. \tag{6.28}$$

Next, we rewrite (6.28) as sums of terms with integrands that satisfy the hypotheses of Theorem 6.1. In order to see how to rewrite the sum, we list the weakly convergent quantities with divergence that satisfy the hypotheses Theorem 6.1. These are $C^\epsilon P^\epsilon\overline{\varphi}$, $C^\epsilon\left(e(\mathbf{r}^\epsilon) - e^\epsilon\right)$, and $C^\epsilon\left(e(\mathbf{u}^\epsilon) - e^\epsilon\right)$. The weakly convergent displacements satisfying the hypotheses of Theorem 6.1 are $\mathbf{v}^{ij,\epsilon} + \overline{e}^{ij}\mathbf{x}$, $\mathbf{r}^\epsilon$, $\mathbf{u}^\epsilon$ and the associated weakly convergent strains are given by $P^\epsilon\overline{e}^{ij}$, $e(\mathbf{r}^\epsilon)$, and $e(\mathbf{u}^\epsilon)$, respectively.

Adding and subtracting e^ϵ and expanding (6.28) yields the nine terms

$$\begin{aligned}
&\int_S \phi C^\epsilon \left(e(\mathbf{u}^\epsilon) - e^\epsilon\right) : e(\mathbf{u}^\epsilon)\, d\mathbf{x} \;-\; \sum_{i,j=1}^{3} \int_S \phi \overline{\varphi}_{ij} C^\epsilon \left(e(\mathbf{u}^\epsilon) - e^\epsilon\right) : P^\epsilon e^{ij}\, d\mathbf{x} \\
&\quad - \int_S \phi C^\epsilon \left(e(\mathbf{u}^\epsilon) - e^\epsilon\right) : e(\mathbf{r}^\epsilon)\, d\mathbf{x} \;-\; \sum_{i,j=1}^{3} \int_S \phi \overline{\varphi}_{ij} C^\epsilon P^\epsilon e^{ij} : e(\mathbf{u}^\epsilon)\, dx \\
&+ \sum_{i,j=1}^{3} \sum_{k,l=1}^{3} \int_S \phi \overline{\varphi}_{ij} \overline{\varphi}_{kl} C^\epsilon P^\epsilon e^{ij} : P^\epsilon e^{kl}\, dx \;+\; \sum_{i,j=1}^{3} \int_S \phi \overline{\varphi}_{ij} C^\epsilon P^\epsilon e^{ij} : e(\mathbf{r}^\epsilon)\, d\mathbf{x} \\
&\quad - \int_S \phi C^\epsilon \left(e(\mathbf{r}^\epsilon) - e^\epsilon\right) : e(\mathbf{u}^\epsilon)\, d\mathbf{x} \;+\; \sum_{i,j=1}^{3} \int_S \phi \overline{\varphi}_{ij} C^\epsilon \left(e(\mathbf{r}^\epsilon) - e^\epsilon\right) : P^\epsilon e^{ij}\, dx \\
&\qquad\qquad + \int_S \phi C^\epsilon \left(e(\mathbf{r}^\epsilon) - e^\epsilon\right) : e(\mathbf{r}^\epsilon)\, d\mathbf{x}. \quad (6.29)
\end{aligned}$$

The limit (6.26) follows on passing to the limit in (6.29) and identifying the limit of each term using Theorem 6.1.

We conclude by establishing the strain bound given in Section 5 and note that the stress bound follows using similar arguments.

Proof. One rewrites the point wise convergence given by (3.10) as

$$\chi_m^\epsilon(\mathbf{x}) e(\mathbf{u}^\epsilon)(\mathbf{x}) = \chi_m^\epsilon(\mathbf{x}) \left(\tilde{P}(\mathbf{x}/\epsilon) e(\mathbf{u}^M)(\mathbf{x}) + e(\tilde{\mathbf{r}})(\mathbf{x}/\epsilon)\right) + z_{sp}^\epsilon(\mathbf{x}), \tag{6.30}$$

where $z_{sp} \to 0$ for almost every $\mathbf{x}$ in S. Substitution of this expansion into the functions J_1 and J_2 and an application of the triangle inequality in the expression corresponding to J_2 gives

$$\begin{aligned}
J_1(\chi_m^\epsilon(\mathbf{x}) e(\mathbf{u}^\epsilon)(\mathbf{x})) &\le (EJ_1)_m(e(\mathbf{u}^M(\mathbf{x}))) + J_1(z_{sp}^\epsilon(\mathbf{x})), \\
J_2(\chi_m^\epsilon(\mathbf{x}) e(\mathbf{u}^\epsilon)(\mathbf{x})) &\le ((EJ_2)_m(e(\mathbf{u}^M(\mathbf{x}))) + J_2(z_{sp}^\epsilon(\mathbf{x}))
\end{aligned} \tag{6.31}$$

and the bounds follows from the continuity of J_1 and J_2.

REFERENCES

[1] J. Aboudi, M. J. Pindera, and S. M. Arnold, *Microstructural optimization of functionally graded composites subjected to thermal gradient via the coupled higher-order theory.* Composites Part B, 28B (1997), pp. 93108.

[2] C. Albert and G. Fernlund, *Spring-in and warpage in curved laminates.* Composites Science and Technology, 62 (2002), pp. 1895–1912.

[3] I. Babuška, *Homogenization and its applications: Mathematical and computational problems,* in Numerical Solution of Partial Differential Equations III, SYNSPADE 1975, B. Hubbard, ed., Academic Press, New York, 1976, pp. 89–116.

[4] I. Babuška, *Soultion to interface problems by homogenization*, SIAM J. Math. Anal. 7 (1976), Part I pp. 603–634, Part II pp. 635–645.

[5] I. Babuška, B. Andersson, P. J. Smith, and K. Levin, *Damage analysis of fiber composites, Part I: Statistical analysis on fiber scale*, Comput. Methods Appl. Engrg., 172 (1999), pp. 27–77.

[6] I. Babuška, R. Lipton, and M. Stüebner, *A generalization of Saint Venant's principle and applications of penetration functions*, preprint.
[7] I. Babuška, T. Strouboulis, and K. Copps, *The design and analysis of the generalized finite element method*, Comput. Meth. Appl. Mech. Engng., 181 (2000), pp.43–69.
[8] A. Bensoussan, J. L. Lions, and G. Papanicolaou, *Asymptotic Analysis for Periodic Structures*, Stud. Math. Appl. 5, North-Holland, Amsterdam, 1978.
[9] A. Bensoussan, J. L. Lions, and G. Papanicolaou, *Boundary layer analysis in homogenization of diffusion equations with Dirichlet conditions on the half space,* Proc. of Intern. Symp. SDE Kyoto, 1976, pp. 21–40.
[10] B. Cox and Q. Yang, *In quest of virtual tests for structural composites*, Science, 314 (2006), pp. 1102–1106.
[11] I. M. Daniel and O. Ishai, Engineering Mechanics of Composite Materials. New York, Oxford University Press, 1994.
[12] G. Dvorak and A. P. Suvorov, *The effect of fiber pre-stress on residual stresses and the onset of damage in symmetric laminates*, Composites Science and Technology, 60 (2000), pp. 1129–1139.
[13] W. E, and B. Engquist, *The heterogeneous multiscale methods,* Commun. Math. Sci., 1 (2003), pp. 87–132.
[14] W. E, P. Ming, and P. Zhang, *Analysis of the heterogeneous multiscale method for elliptic homogenization problems*, J. Amer. Math. Soc., 18, (2004), pp. 121-156.
[15] Y. R. Efendiev, T. Y. Hou and X. Wu, *Convergence of a nonconforming multiscale finite element method* ,J Comput. Phys. 37 (2000), pp. 888-910.
[16] C. Eringen, *Microcontinuum Field Theories I: Foundations and Solids*, Springer-Verlag, New York, 1999.
[17] D. Faraco, *Milton's conjecture on the regularity of isotropic equations*, Ann. Inst. H. Poincare, 20 (2003), pp. 899–909.
[18] J. Fish and Z. Yuan, *Multiscale enrichment based on partition of unity* Int. J. Mum. Meth. Engr., 62 (2005), pp. 1341-1359.
[19] G. A. Francfort and F. Murat, *Homogenization and optimal bounds in linear elasticity,* Arch. Rat. Mech. Anal., 94 (1986), pp. 307–334.
[20] J. H. Gosse and S. Christensen, *Strain invariant failure criteria for polymers in composite materials*, AIAA, 1184 (2001), p. 11.
[21] V. H. Hoang and C. Schwab, *High-dimensional finite elements for elliptic problems with multiple scales,* Multiscale Model. Simul., 3 (2005), pp. 168–194.
[22] T. Y. Hou and X. H. Wu, *A multiscale finite element for elliptic problems in composite materials and porous media*, J. Comput. Phys., 134 (1997), pp. 169–189.
[23] T. Y. Hou, X. H. Wu and Z. Cai, *Convergence of a multiscale finite element method for elliptic problems with rapidly varying coefficients*, Math. Comp., 68 (1999), pp. 913–943.
[24] T. Hughes, G. Feijoo, L. Mazzei, and J. Quincy, *The variational multiscale method: A paradigm for computational mechanics,* Comput. Meth. Appl. Mech. Engng., 166 (1999), pp.913–943.
[25] P. Hutapea, F. G. Yuan, and N. J. Pagano, *Micro-stress prediction in composite laminates with high stress gradients,* Int. J. Solids Structures, 40 (2003), pp. 2215–2248.
[26] E. V. Iarve, *Spline variational three dimensional stress analysis of laminated composite plates with open holes,* Int. J. of Solids Structures, 33 (1996), pp. 2095–2117.
[27] P. Ifju, D. Myers, and W. Schultz, *Residual stress and thermal expansion of graphite epoxy laminates subjected to cryogenic temperatures*, Composites Science and Technology, 66 (2006), pp. 2449–2455.
[28] C. Kassapoglou and P. A. Lagace, *An efficient method for the calculation of interlaminar stresses in composite materials*, J. Appl. Mech., 53 (1986), pp. 744–750.
[29] R. B. Kellogg, *Singularities in interface problems*, in Numerical Solution of Partial Differential Equations II, B. Hubbard, ed., Academic Press, New York, 1971, pp. 351–400.
[30] A. G. Kolpakov, *Effect of influence of initial stresses on the homogenized characteristics of composites,* Mechanics of Materials, 37 (2005), pp. 840–854.

[31] F. Leonetti and V. Nesi, *Quasiconformal solutions to certain first order systems and the proof of a conjecture of G. W. Milton*, J. Math. Pures. Appl. 76 (1997), pp. 109–124.

[32] R. Lipton, *Assessment of the local stress state through macroscopic variables,* Phil. Trans. R. Soc. Lond. A, 361 (2003), pp. 921–946.

[33] R. Lipton, *Bounds on the distribution of extreme values for the stress in composite materials,* J. Mech. Phys. Solids, 52 (2004), pp. 1053–1069.

[34] R. Lipton, *Homogenization and field concentrations in heterogeneous media,* SIAM J. on Math. Analysis, 38 (2006), pp. 1048–1059.

[35] S. V. Lomov, G. Huysmans, Y., Luo, R. S. Parnas, A. Prodromou, I. Verpoest, and F. R. Phelan, *Textile composites: modeling strategies,* Composites: Part A, 32 (2001), pp.1379-1394.

[36] G. W. Milton, *Modelling the properties of composites by laminates*, in Homogenization and Effective Moduli of Materials and Media, J. Ericksen, D. Kinderleher, R.V. Kohn, J.L. Lions, eds., IMA Volumes in Mathematics and Its Applications 1, Springer Verlag, New York, 1986, pp. 150–174.

[37] S. Moskow and M. Vogelius, *First order correctors to the homogenized eigenvalues of a periodic composite medium. A convergence proof.,* Proc. Roy. Soc. Edinburgh Sect. A 127 (1997), pp. 1263–1299.

[38] M. Neuss-Radu, *The failure of uniform exponential decay for boundary layers,* Multiscale Problems in Science and Technology (Dubrovnik 2000). Springer Berlin, 2002, pp. 243–250.

[39] J. T. Oden and K. Vemaganti, *Estimation of local modeling error and goal oriented modeling of heterogeneous materials; part I. Error estimates and adaptive algorighms,*, Journal of Computational Physics, 164 (2000), pp. 22–47.

[40] J. T. Oden, K. Vemaganti, and N. Moës, *Hierarchical modeling of heterogeneous solids*, Comput. Methods Appl. Mech. Engng., 172 (1999), pp. 3–25.

[41] J. T. Oden and T. I. Zohdi, *Analysis and adaptive modeling of highly heterogeneous elastic structures*, Comput. Methods Appl. Mech. Engng., 148 (1997), pp. 367–391.

[42] N. J Pagano, G. A. Schoeppner, R. Kim, and F. L. Abrams, , *Steady-state cracking and edge effects in thermo-mechanical transverse cracking of cross-ply laminates,* Comp. Sci. and Tech., 58 (1998), pp. 1811–1825.

[43] G. Paşa, *Convergence et correctures pour des équations avec terrmes libres oscillants rapidement*, C. R. Acad. Sc. Paris Ser. I Math 299 (1984), pp. 1037–1039.

[44] P. Raghaven, S. Moorthy, S. Ghosh, and N.J. Pagano, *Revisiting the composite laminate problem with an adaptive multi-level computational model*, Comp. Sci. Tech., 61 (2001), pp. 1017–1040.

[45] E. Sanchez-Palencia, *Nonhomogeneous Media and Vibration Theory.* Lecture Notes in Physics, 127, Springer-Verlag, New York, 1980.

[46] T. Strouboulis, L. Zhang and I. Babuška,*p-version of the generalized FEM using mesh-based handbooks*, Int. J. Num. Meth. Engr., 60 (2004), pp. 1639-1672.

[47] A. P. Suvorov and G. Dvorak, *Optimized fiber pre-stress for reduction of free edge stresses in composite laminates*, Int. J. of Solids Structures, 38 (2001), pp. 6751–6786.

[48] T. I. Zhodi, J. T. Oden, and G. J. Rodin, *Hierarchical modeling of heterogeneous bodies,* Comput. Methods Appl. Engng., 138 (1996), pp. 273–298.

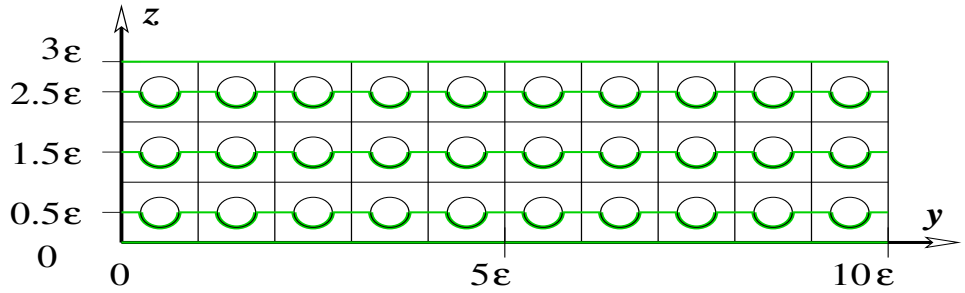

FIG. 5.1. *The 4 different paths inside the 0 degree ply used to compare stress invariants*

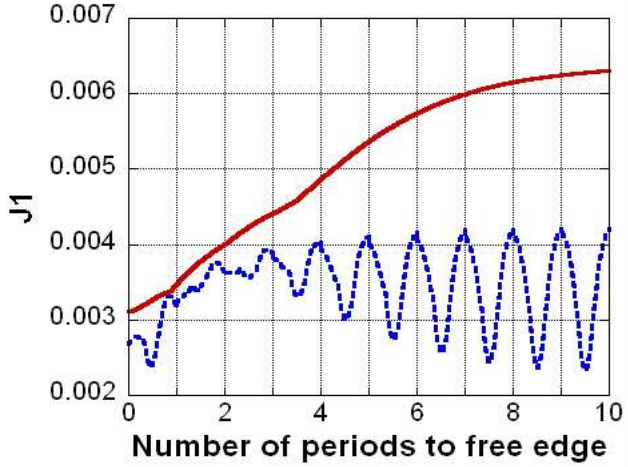

FIG. 5.2. *Comparison of J_1 and $(EJ_1)_1$ in 0 degree ply 3.0 fiber diameters above the interface.*

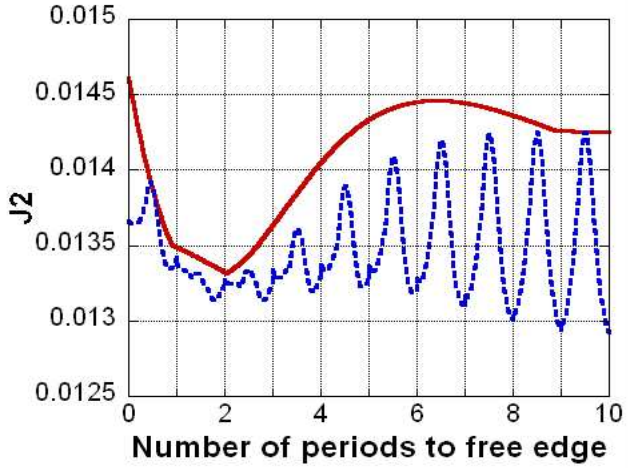

FIG. 5.3. *Comparison of J_2 and $(EJ_2)_1$ in 0 degree ply 3.0 fiber diameters above the interface.*

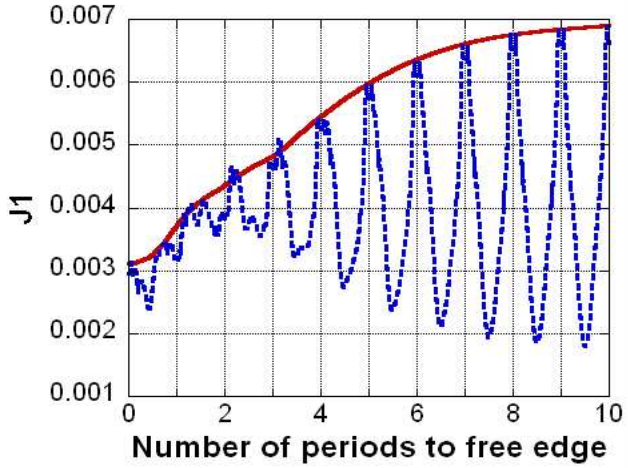

FIG. 5.4. *Comparison of J_1 and $(EJ_1)_1$ in 0 degree ply 2.5 fiber diameters above the interface.*

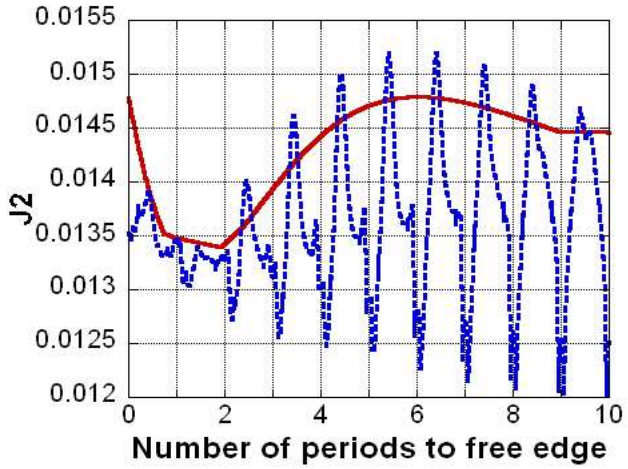

FIG. 5.5. *Comparison of J_2 and $(EJ_2)_1$ in 0 degree ply 2.5 fiber diameters above the interface.*

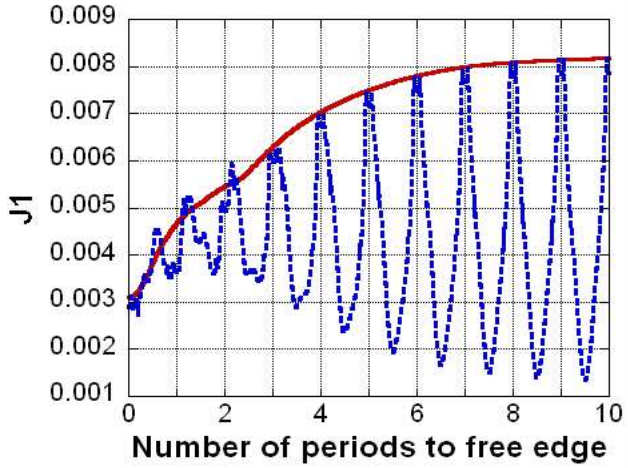

FIG. 5.6. *Comparison of J_1 and $(EJ_1)_1$ in 0 degree ply 1.5 fiber diameters above the interface.*

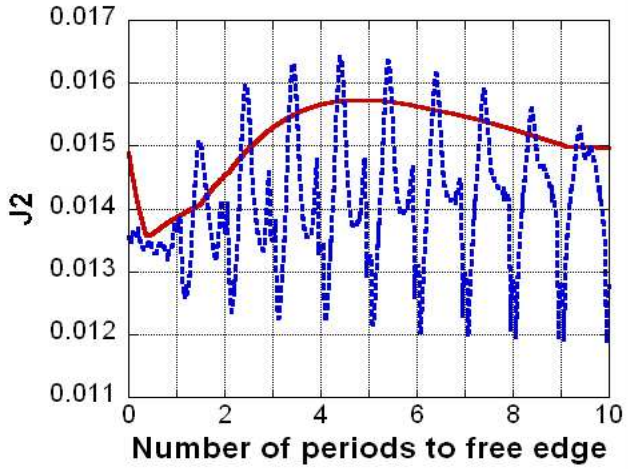

FIG. 5.7. *Comparison of J_2 and $(EJ_2)_1$ in 0 degree ply 1.5 fiber diameters above the interface.*

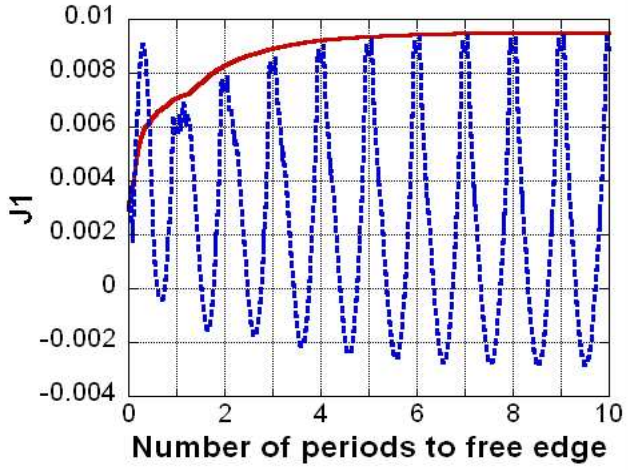

FIG. 5.8. *Comparison of J_1 and $(EJ_1)_1$ in 0 degree ply 0.5 fiber diameters above the interface.*

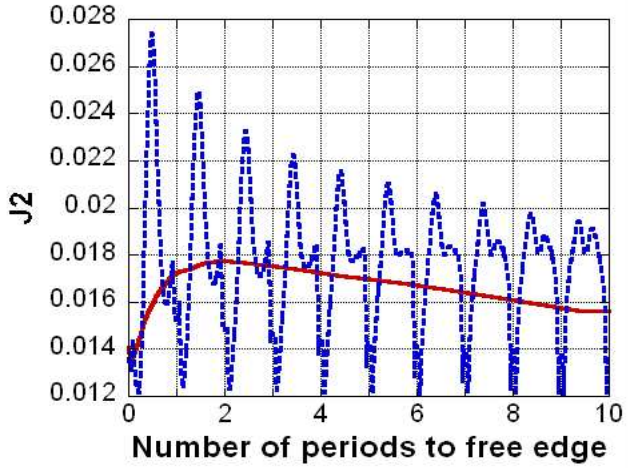

FIG. 5.9. *Comparison of J_2 and $(EJ_2)_1$ in 0 degree ply 0.5 fiber diameters above the interface.*

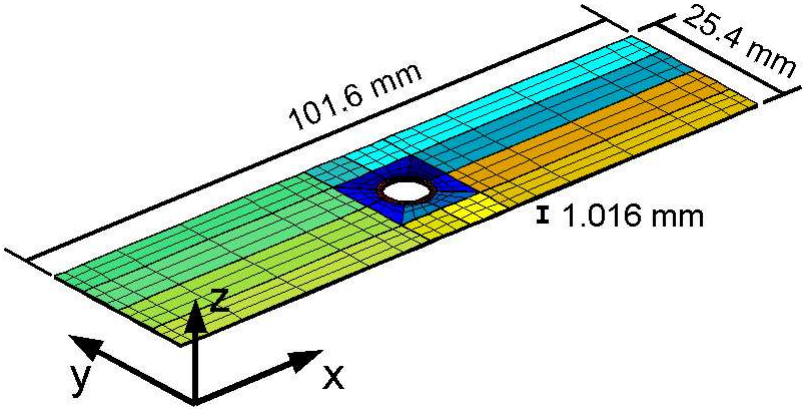

FIG. 5.10. *An open hole eight ply laminate*

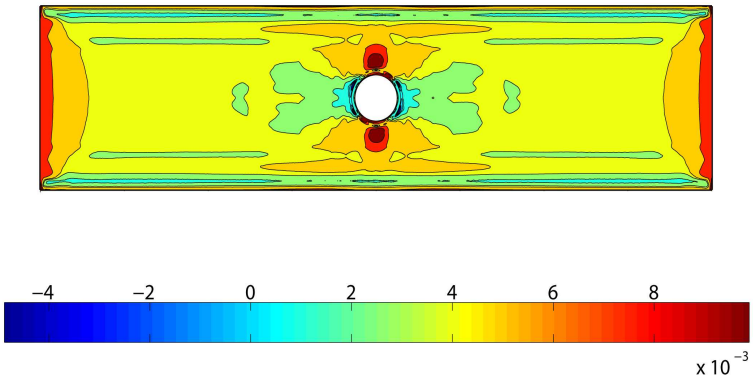

FIG. 5.11. *Bound on the local strain in the 0 degree ply without prestress*

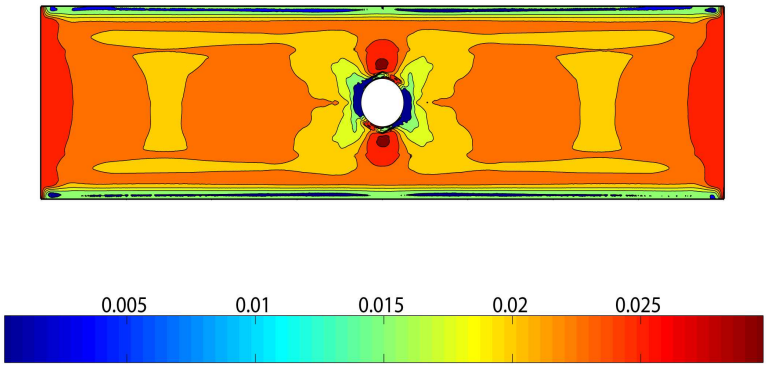

FIG. 5.12. *Bound on the local strain in the 0 degree ply with prestress*

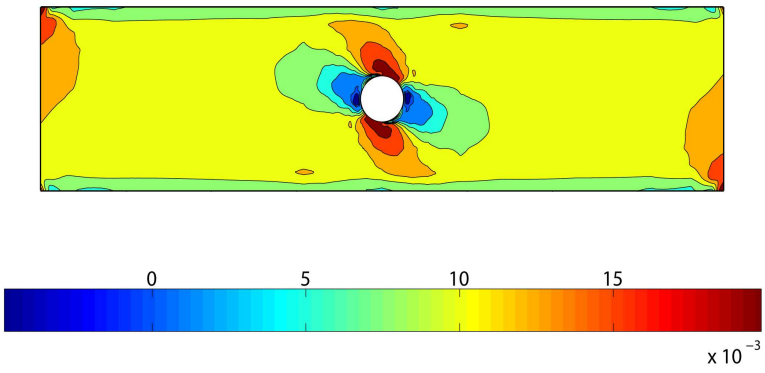

FIG. 5.13. *Bound on the local strain in the 45 degree ply without prestress*

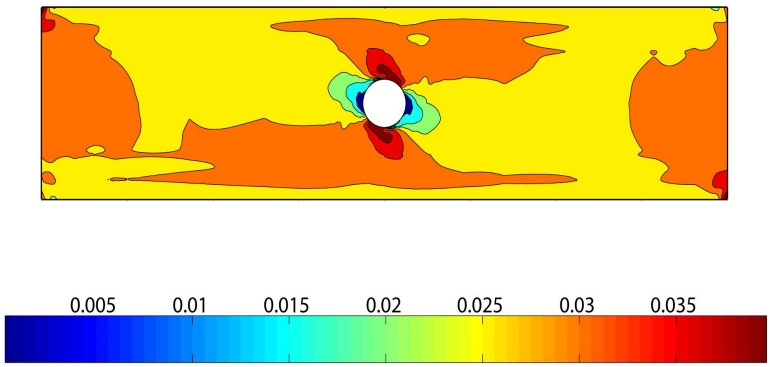

FIG. 5.14. *Bound on the local strain in the 45 degree ply with prestress*

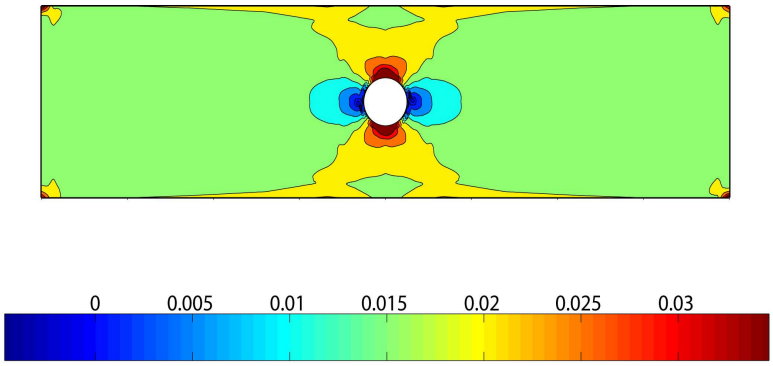

FIG. 5.15. *Bound on the local strain in the 90 degree ply without prestress*

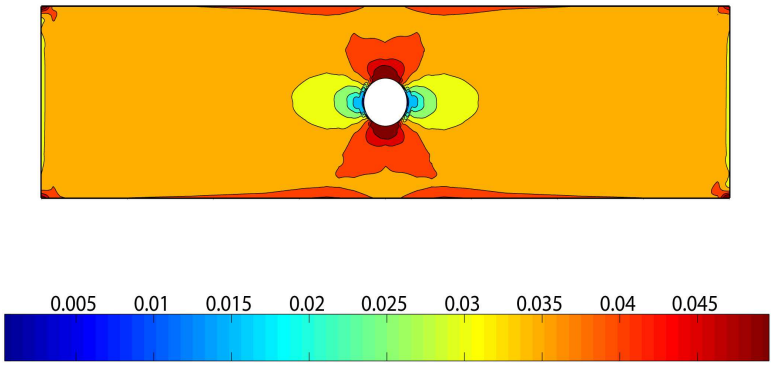

FIG. 5.16. *Bound on the local strain in the 90 degree ply with prestress*